



Resolving *P*-wave travel-time anomalies using seismic array observations of oceanic storms

Jian Zhang^{*}, Peter Gerstoft, Peter M. Shearer

Scripps Institution of Oceanography, University of California, San Diego 9500 Gilman Drive, La Jolla, CA 92093-0238, USA

ARTICLE INFO

Article history:

Received 5 October 2009
Received in revised form 8 February 2010
Accepted 9 February 2010
Available online 6 March 2010

Editor: R.D. van der Hilst

Keywords:

P-wave
microseism
travel-time anomaly
body-wave tomography
storm

ABSTRACT

Array analysis of seismic noise has the potential to be very useful in improving body-wave tomography of Earth structure, just as noise cross-correlation methods have recently proven successful in surface-wave tomography. Beamforming of seismic noise recorded in southern California reveals *P*-wave arrivals from distant storms in open oceans. In this case, the noise can be processed using cross-correlation among different station pairs and optimal *P*-wave relative arrival times can be estimated using the same approach traditionally used to analyze earthquake arrival times.

Using three storms in the Gulf of Mexico, the Western Pacific (near Japan), and the South Pacific (near Fiji) respectively, we demonstrate that travel-time anomalies can be obtained from *P* waves generated by a distant storm, and that they are similar to those obtained from using an earthquake close to the storm. Our results suggest using oceanic storms as additional seismic sources for resolving *P*-wave travel-time anomalies.

© 2010 Elsevier B.V. All rights reserved.

1. Introduction

Since the pioneering studies by K. Aki et al. in the mid 1970s (Aki et al., 1976; Husebye et al., 1976; Aki et al., 1977), teleseismic *P*-wave travel-time anomalies derived from using earthquakes have been providing the data for inferring three-dimensional (3-D) velocity heterogeneities beneath seismic networks or arrays, i.e., regional/local body-wave tomography. Besides advances in algorithms, better data can always improve tomography results, which has in part come from the deployment of additional instruments, the use of multiple phases, and more accurate arrival-time picks. However, inhomogeneous data coverage, particularly the absence of both earthquakes and seismic instruments in many open oceans, has long been a challenge for seismic imaging. For teleseismic body-wave tomography, this may result in poor coverage of certain directions. Studies of phase delay times across southern California, for instance, have been hampered by azimuthal gaps to the south and northeast (e.g., Humphreys and Clayton, 1990; Polet, 2007). Thus, additional seismic sources, if available, could help fill azimuthal gaps in the data.

An alternative to earthquakes (and/or controlled sources) is storms. Hiding in microseisms there are non-pulse-like yet coherent *P* waves that are generated by oceanic storms, which can be revealed by seismic array observations. *P* waves from storms have been reported as early as in the late 1960s (Toksoz and Lacoss, 1968; Lacoss et al., 1969; Haubrich and

McCamy, 1969), but then received little attention until Hurricane Katrina “hit” California and Gerstoft et al. (2006a, see also Fig. 1) were able to characterize and back-project the hurricane-generated *P* waves with beamforming of seismic noise recorded at the Southern California Seismic Network (SCSN). These *P* waves are observable in the entire secondary microseism band but are often strongest in the upper secondary part (~0.15–0.3 Hz). Modern array techniques now have allowed the accumulation of more observations of *P* waves that can be associated with sea states and even specific storms (Gerstoft et al., 2008; Koper and de Foy, 2008; Landes et al., 2010; Koper et al., 2010; Zhang et al., 2009). In Fig. 2, for example, the source regions of *P*-wave microseisms observed at the SCSN during September 1–9, 2006 can be traced by the peak power locations of the beamformer outputs. The track of the *P*-wave source regions agrees well with that of Super Typhoon Ioke, clearly indicating that these *P* waves originate from oceanic storms.

Noise cross-correlation (NCC) of coherent *P* waves such as those observed in Gerstoft et al. (2006a and 2008) at the SCSN can therefore be used to measure the time lag of *P* arrivals between a pair of stations, and thus lead to estimates of relative *P*-wave arrival times across an array from distant noise sources. These relative arrival times, if accurate enough, contain information about 3-D seismic velocity anomalies under the array. This suggests that it may be possible to supplement earthquake data with *P*-wave microseisms from areas of active storms, for performing regional body-wave tomography of crust and upper-mantle structure. It should be noted that NCC processing has recently become popular in extracting Green's functions from seismic noise (Shapiro and Campillo, 2004; Snieder, 2004; Wapenaar, 2004; Sabra et al., 2005a), which has made possible the use of ambient noise for surface-wave tomography (Shapiro

^{*} Corresponding author. Tel.: +1 858 822 4095; fax: +1 858 534 7641.
E-mail address: jianz@ucsd.edu (J. Zhang).

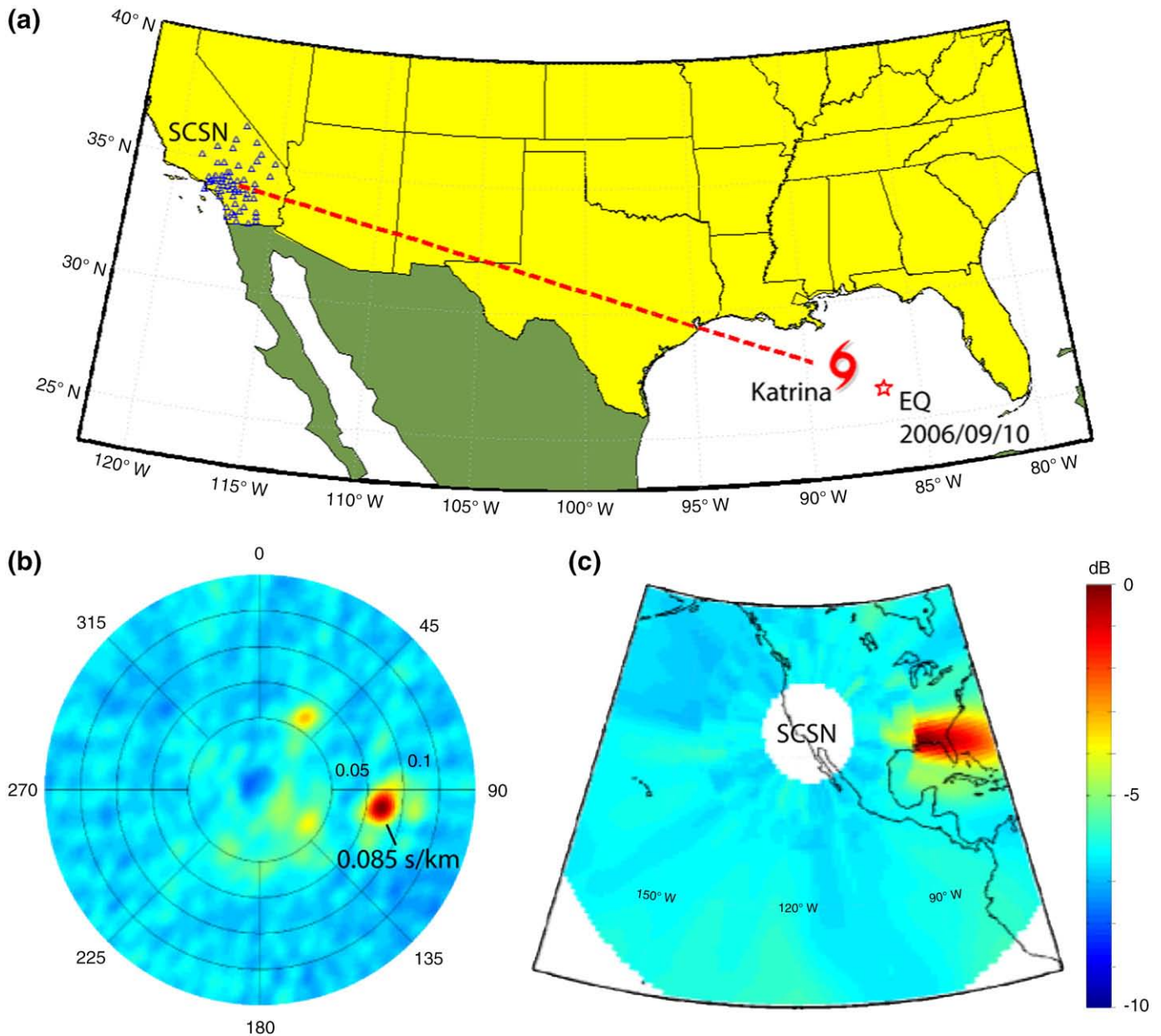


Fig. 1. Hurricane Katrina. (a) Locations of the Southern California Seismic Network (SCSN), Hurricane Katrina (schematic) on August 28, 2005, and an Mw 5.9 earthquake on September 10, 2006. The dashed line indicates the projected great circle path (27° in distance) of the P waves from Katrina to southern California. (b) Azimuth–slowness beam of 0.19-Hz vertical-component seismic noise recorded by the SCSN, showing a P -wave arrival (0.085 s/km, i.e., 11.8 km/s) from a back-azimuth of 100° ; (c) Source region of the P waves obtained by back-projecting the beam in (b).

et al., 2005; Sabra et al., 2005b; Yao et al., 2006; Kang and Shin, 2006; Yang et al., 2007; Moschetti et al., 2007; Lin et al., 2007, 2008; Yang et al., 2008; Yao et al., 2008; Liang and Langston, 2008; Zheng et al., 2008). However, as discussed by a few studies (Gerstoft et al., 2006b; Stehly et al., 2006; Yang and Ritzwoller, 2008; Tsai, 2009; Yao and van der Hilst, 2009), one should be careful in relating the NCC time series to the Green's function between a station pair when the distribution of noise sources is uneven. In cases where the noise field is dominated by strongly directional sources, such as P waves from storms, the phase delay times from the NCC peaks are source direction dependent.

We demonstrate in this paper that the delay times measured from NCC processing of P waves from storms, which are “bias events” in terms of extracting Green's functions for surface-wave tomography, can in fact provide travel-time anomaly information for teleseismic body-wave tomography. In particular, we identify and characterize the direct P -wave arrivals observed at the SCSN from three storms

(see Figs. 1 and 3) – Hurricane Katrina in the Gulf of Mexico, Super Typhoon Ioke in the Western Pacific (near Japan), and a storm in the South Pacific (near Fiji). We then validate the basic approach by following VanDecar and Crosson (1990) to obtain relative arrival times. For each storm we calculate the P -wave travel-time anomalies beneath southern California, and compare the result with that derived from using an earthquake close to the storm. It is noteworthy that these storms are at relatively great distances from the SCSN (~ 27 – 78°), so that the P -wave arrivals can be approximated as plane waves, just as is commonly done when using earthquakes in teleseismic tomography.

2. Data processing and analysis

Our analysis starts with array beamforming for identifying P -wave arrivals in seismic noise, as well as their sources. We use continuous

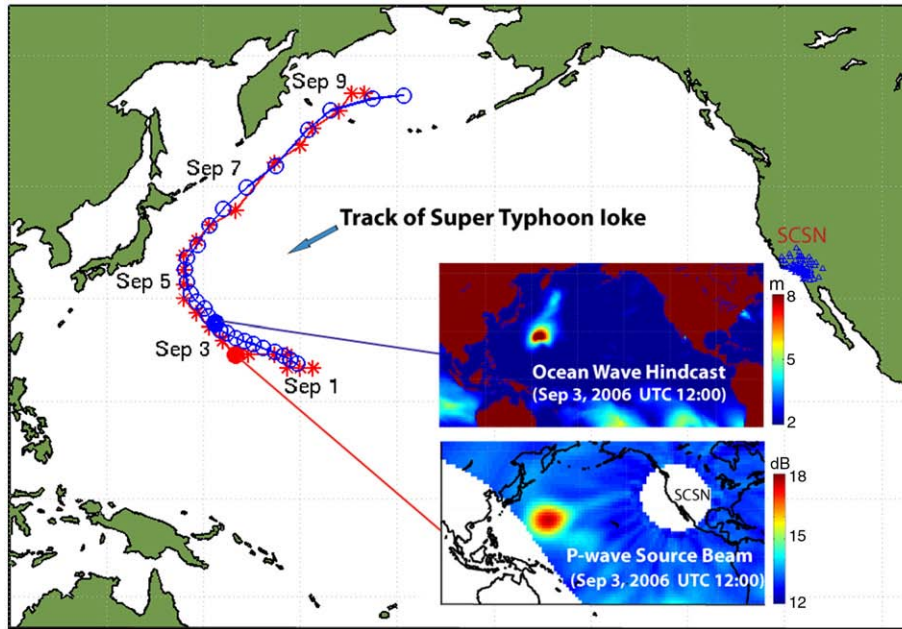


Fig. 2. Tracks of the *P*-wave source regions (stars) and Super Typhoon Ioke (circles). The track points of the peaks of source regions are derived from source beamforming using the SCSN seismic data (every 6 h, and limited by the 2° resolution). The best track of Super Typhoon Ioke is based on the observations and analysis of the Japan Meteorological Agency and available from [http://agora.ex.nii.ac.jp/digital-typhoon/]. The inserts show both a map of the ocean wave hindcast and a map of the *P*-wave source region, sampled for September 3, 2006, UTC 12:00.

vertical-component data (sampled at 1 s) recorded at the SCSN for the time-window covering Hurricane Katrina’s landing (August 28–29, 2005), and also for the whole year of 2006. Note that a 1-s sample rate allows faster beamforming yet is sufficient for identifying coherent microseisms. The data are truncated to no more than half of the daily standard deviations to mitigate contamination from occasional large-amplitude events (e.g., earthquakes). Beamforming is done within each 3 h window for each 0.02–Hz bandwidth (details in Gerstoft et al., 2006a, 2008). Fig. 1b shows an example of the azimuth–slowness beam at 0.19 Hz during Hurricane Katrina, which indicates a *P*-wave arrival coming from 100° and with a horizontal phase slowness of 0.085 s/km, i.e., 11.8 km/s. By comparing the beamformed source regions with the ocean wave hindcast data (Tolman, 2005), many *P*-wave events in the microseisms during 2006 are found to be due to specific storms (see Figs. 2 and 3 for example). These storms, plus Katrina, serve as candidates for the NCC processing. For each storm we then compute the NCC time series (time lags up to 400 s, using data sampled at 0.05 s) among all station pairs and construct range-time plots to show propagating waves. Note that the ranges are the station separations projected along the storm direction, obtained from the beamformer output. We use a passband of 0.18–0.25 Hz for the NCC processing, in order to focus on the *P*-wave microseisms.

A typical storm suitable for travel-time analysis should reach a sufficient signal-to-noise ratio (SNR) for its NCC peaks, so as to show up as an apparent propagating wave associated with its *P*-wave speed from beamforming. We define the SNR as the ratio of the peak in the *P* arrival window (+/–20 s of the plane-wave arrival as derived from beamforming) to the standard deviation for a “noise-only” window (300–400 s of an NCC time series). For example in Fig. 4b, a propagating *P* wave from Katrina can be clearly seen in the range-time representation of the NCC time series of 400 station pairs (only a fraction is shown) with a SNR above 9, calculated for 1-day data (UTC 18:00 August 28 to UTC 18:00 August 29, 2005). Besides the SNR criterion, we apply a cutoff range over 100–400 km, given that there is an ambiguity between *P*-wave and coastal surface-wave arrivals at shorter ranges, and that times at longer ranges may not be well represented by the plane-wave assumption. In addition to Katrina, we have collected two more storms in 2006 (as mentioned in Section 1,

see Fig. 3) for performing relative arrival-time measurements. For each of them, the *P*-wave delay time of each station pair is simply the offset of the maximum of the NCC function, e.g., see the dots in Fig. 4b. Instead of the 1-s data used for the beamforming analysis, however, here we use the data sampled at 0.05 s for picking the peak times of the NCC functions, in order to obtain the delay-time estimates with a higher precision. Moreover, we select only delay-time measurements within +/–2 s relative to the plane-wave arrival times approximated by the beamforming result. This criterion can remove large outliers, yet still covers the magnitude of typical regional travel-time anomalies.

Our approach of determining travel-time anomalies follows VanDecar and Crosson (1990). We optimize relative arrival-time estimates through using least squares to solve an overdetermined system of delay-time equations, assuming that errors in the NCC-derived delay times are primarily random in nature. For station pairs with a sufficient SNR, we generate equations given by $t_i - t_j = \Delta t_{ij}$. This system is expressed as $A \cdot t = \Delta t$. A is a $M \times N$ sparse coefficient matrix, where M is the number of equations and N is the number of stations. The i th and j th columns of A in a row associated with Δt_{ij} are 1 and –1 respectively, while the other columns are zeros, and we add the constraint equation $\sum t_i = 0$ to force the arbitrary mean of the relative arrival times to be zero. Note that $N < M < (N - 1) \cdot N/2 + 1$, as only the pairs with SNR above a certain criterion are used. Thus the system takes the form

$$\begin{bmatrix} 1 & -1 & 0 & 0 & \dots & 0 \\ 1 & 0 & -1 & 0 & \dots & 0 \\ 1 & 0 & 0 & -1 & \dots & 0 \\ & \dots & \dots & \dots & \dots & \dots \\ 1 & 0 & 0 & 0 & \dots & -1 \\ 0 & 1 & -1 & 0 & \dots & 0 \\ 0 & 1 & 0 & -1 & \dots & 0 \\ & \dots & \dots & \dots & \dots & \dots \\ 0 & 1 & 0 & 0 & \dots & -1 \\ & \dots & \dots & \dots & \dots & \dots \\ 1 & 1 & 1 & 1 & \dots & 1 \end{bmatrix} \cdot \begin{bmatrix} t_1 \\ t_2 \\ t_3 \\ t_4 \\ \vdots \\ t_N \end{bmatrix} = \begin{bmatrix} \Delta t_{12} \\ \Delta t_{13} \\ \Delta t_{14} \\ \vdots \\ \Delta t_{1N} \\ \Delta t_{23} \\ \Delta t_{24} \\ \vdots \\ \Delta t_{2N} \\ 0 \end{bmatrix}$$

A standard least-squares fit $t^{\text{est}} = A^+ \cdot \Delta t$, where the pseudoinverse $A^+ = (A^T \cdot A)^{-1} \cdot A^T$, can be found by applying singular value

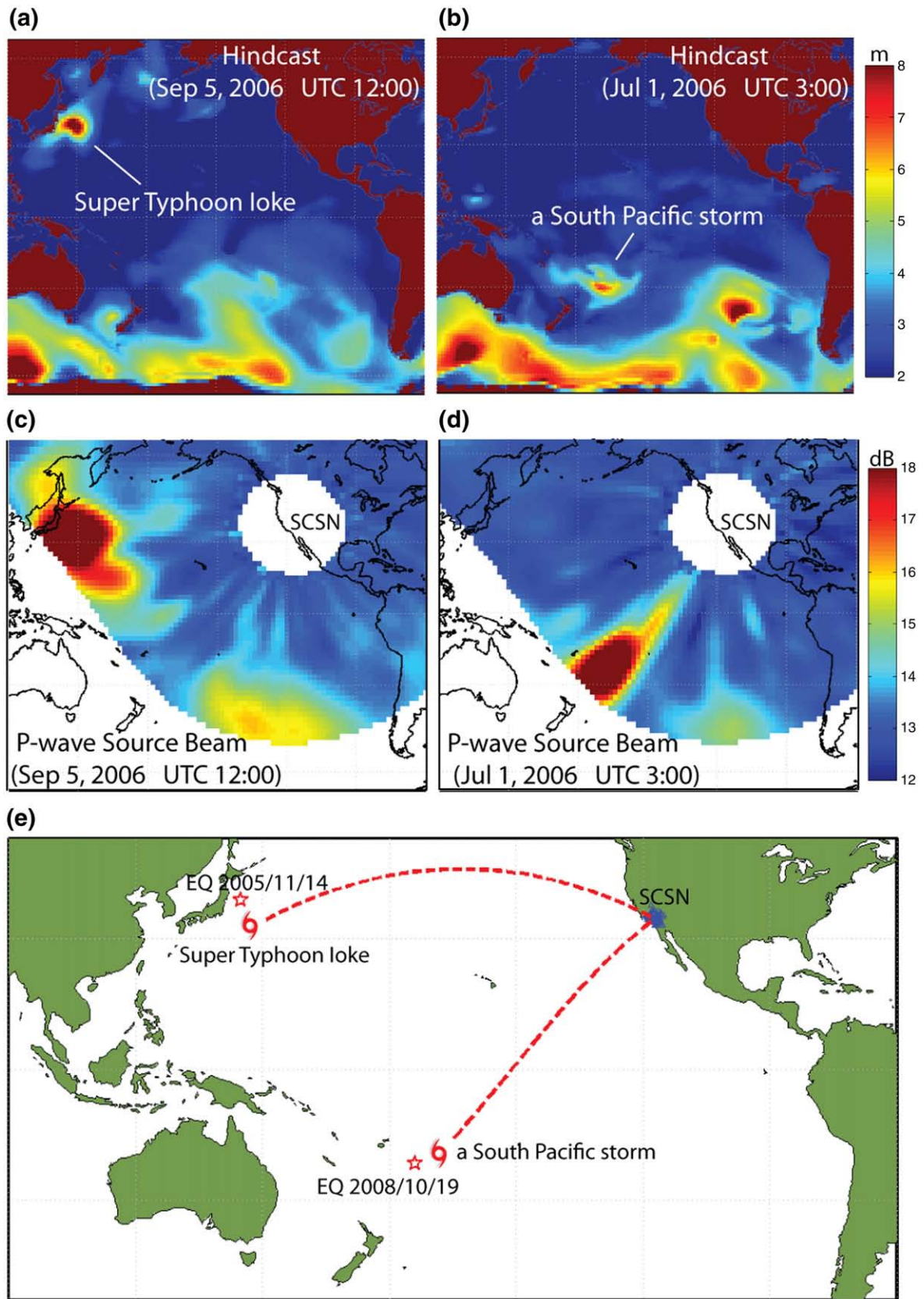


Fig. 3. Maps showing the two storms in 2006 and the two nearby earthquakes. (a) Hindcast of the significant wave height observed on September 5, 2006, UTC 12:00. (b) Hindcast on July 1, 2006, UTC 3:00. (c) P-wave source beam derived from microseisms recorded at the SCSN on September 5, 2006, at the same time as for (a). (d) P-wave source beam on July 1, 2006, at the same time as for (b). Super Typhoon Ioke in the Western Pacific can be clearly tracked in both (a) and (c), as well as a South Pacific storm in (b) and (d). (e) Locations of the SCSN, Super Typhoon Ioke (schematic), an Mw 7.0 earthquake on November 14, 2005, a South Pacific storm (schematic), and an Mw 6.9 earthquake on October 19, 2008. The dashed lines indicate the great circle paths of the P waves from the storms to the SCSN.

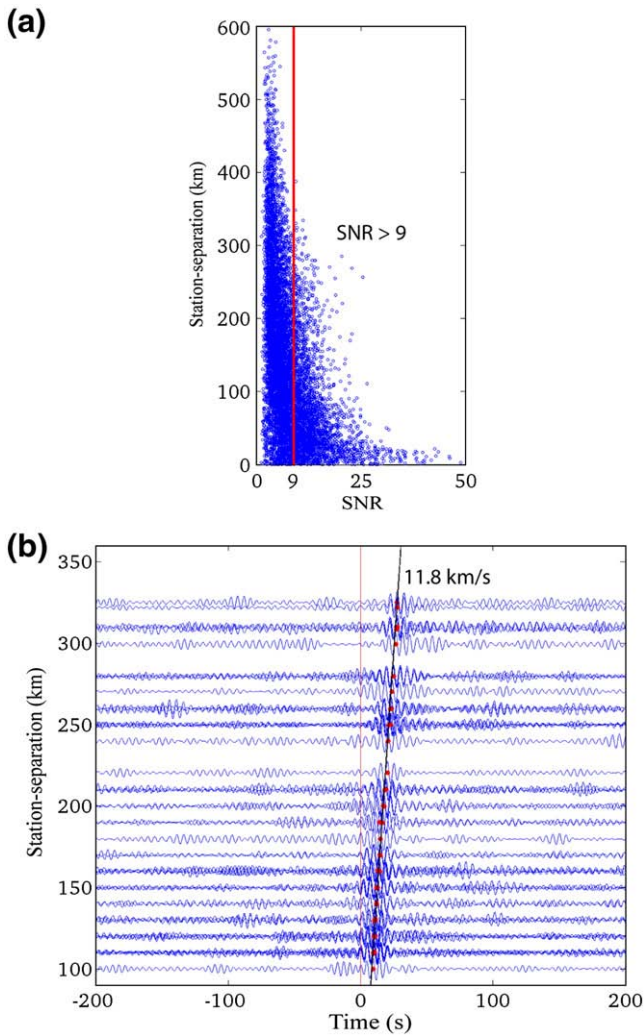


Fig. 4. Delay-time measurements from using Hurricane Katrina. (a) SNR vs. station-separation (projected along 100°). The vertical line indicates a SNR of 9. (b) Range-time representation of the noise cross-correlation (NCC) time series for sample station pairs with SNR > 9. Dots in (b) mark the delay-time measurements (offsets of the NCC peaks) of *P* waves for each pair of stations. The thick line indicates an 11.8 km/s plane wave.

decomposition (SVD) and truncating small singular values. We repeat the procedure by removing outliers, i.e., the station pairs with a residual over 3 times the standard deviation of all residuals. Typically a stable solution is obtained after 4 iterations. For large systems in which SVD becomes computationally impractical, iterative methods such as the conjugate gradient algorithm LSQR of Paige and Saunders (1982) can be used to find the solution t^{est} .

We have found that the equation residuals $res_{ij} = \Delta t_{ij} - (t_i^{est} - t_j^{est})$ derived from the best-fitting solutions are nearly Gaussian-type distributed. An example is shown in Fig. 5a for the Katrina result. This suggests that the least-squares solutions can provide reasonable estimates of the relative arrival times. In addition, to evaluate the accuracy of the least-squares estimates of the relative *P* arrival times using seismic noise, we perform a statistical resampling analysis (i.e., the “bootstrap” method, Efron, 1982; Shearer, 1997; Waldhauser and Ellsworth, 2000) by replacing the equation residuals with a randomly chosen set of residuals from the best fitting solutions. The process is then repeated 200 times, and the standard deviation of these bootstrap outputs provides an estimate of the timing uncertainty for each station. Fig. 5b shows, for an example of the Katrina processing, that a level of 0.1 s in timing errors can be reached, which should be sufficient for resolving typical *P*-wave travel-time anomalies on the order of 1 s.

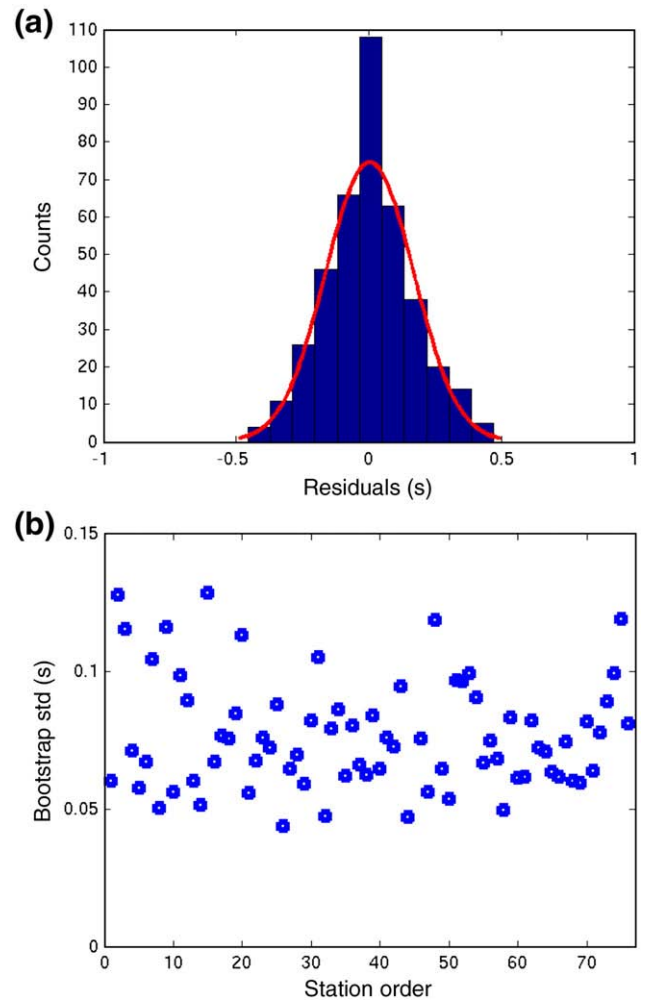


Fig. 5. Least-squares residuals and uncertainty estimation in differential times obtained from using Hurricane Katrina. (a) Histogram of equation residuals derived from the best-fitting solutions, showing a Gaussian-like distribution. The curve indicates a fitted normal distribution. (b) Bootstrap-resampling derived timing uncertainties of the *P*-wave relative arrival times for each station.

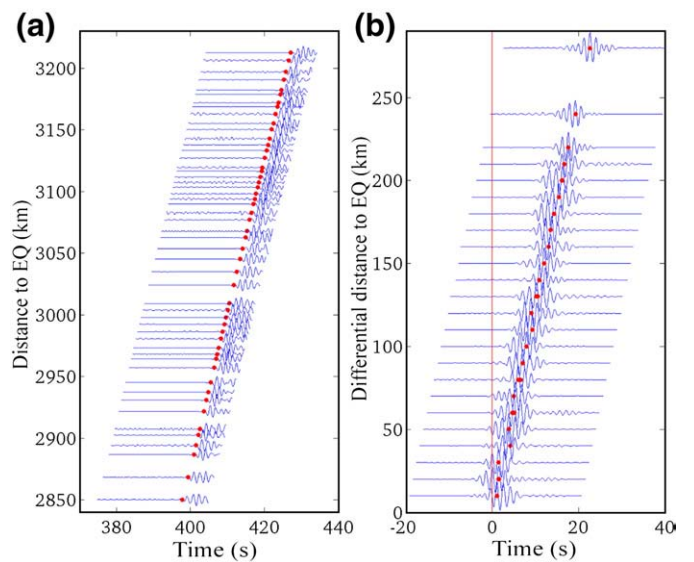


Fig. 6. Delay-time measurements from using EQ 2006/09/10. (a) Waveforms of the *P*-wave arrivals at the sample SCSN stations from EQ 2006/09/10. Dots mark the *ak135*-predicted travel times at each station. (b) Range-time representation of the earthquake waveform cross-correlation time series for sample station pairs. Dots mark the delay-time measurements (offsets of the cross-correlation peaks).

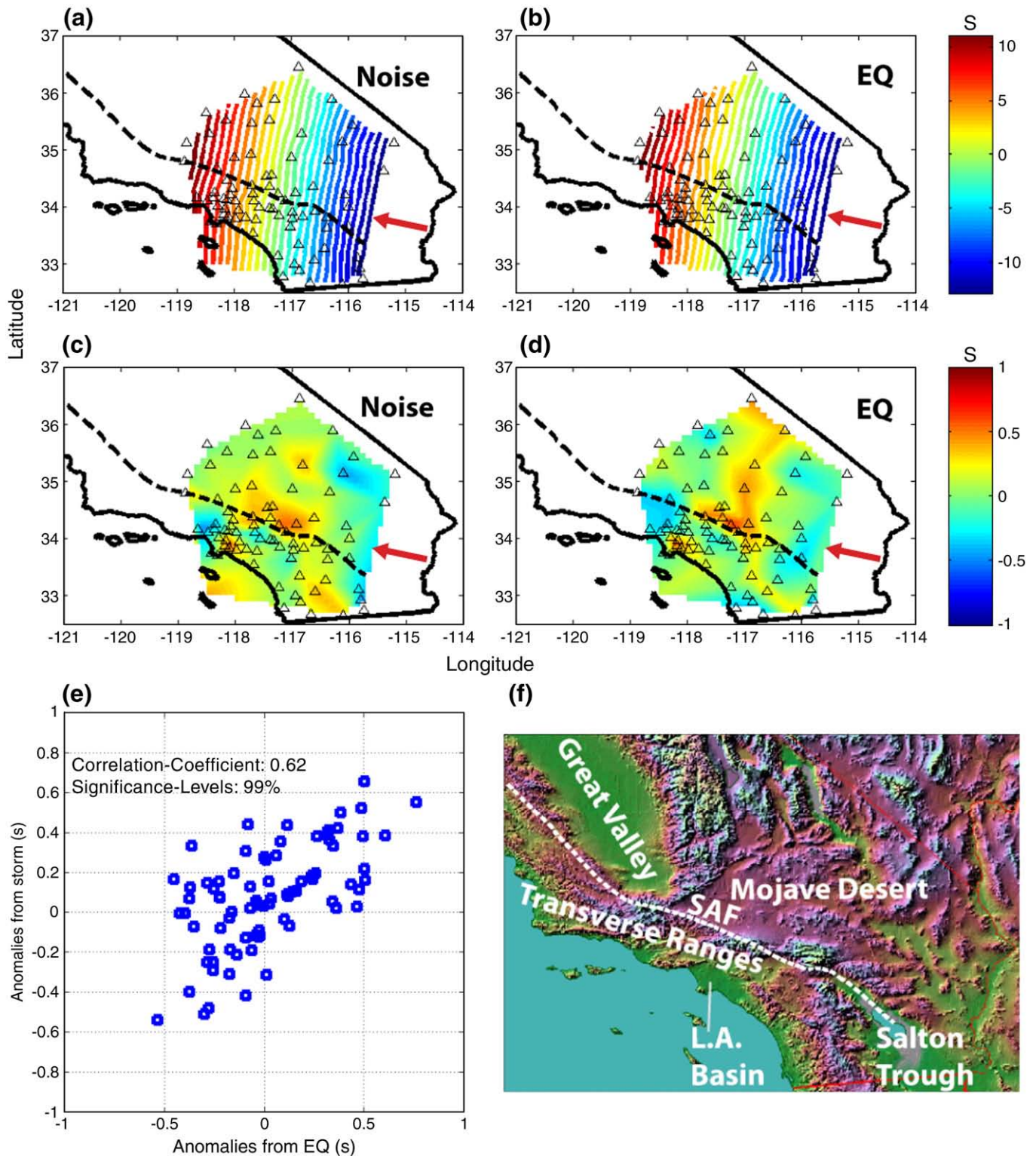


Fig. 7. Relative *P* arrival times in southern California as determined by using (a) Katrina, compared with those as determined by using (b) EQ 2006/09/10. See Fig. 1a for the storm and earthquake locations. Maps are also shown for *P* travel-time anomalies obtained from (c) subtracting a plane wave (100° in back-azimuth and 11.8 km/s in speed) from the NCC-derived arrival times in (a), compared with those obtained from (d) subtracting the *ak135*-predicted arrivals of EQ 2006/09/10 from the EQ-derived arrival times in (b). The used stations (triangles) and the San Andreas Fault (SAF) trace (dashed) are indicated in the maps. Arrows indicate the direction of the *P*-wave arrivals. (e) Scatter plot of EQ-determined anomalies vs. noise-determined anomalies at all common stations. (f) A topographic map showing the basic geological features of southern California.

3. Comparison of the results from using storms and earthquakes

To demonstrate the accuracy of the approach for using *P*-wave noise from the three storms, for each one we find an appropriate earthquake that is close to the storm and big enough to produce clear

P pulses at the SCSN stations. We process the earthquake data in the same manner as described in Section 2. The principal difference to the NCC processing is that the cross-correlation using the earthquake signals takes advantage of the waveform similarity of the direct *P* arrivals in a short time-window, unlike using non-pulse-like noise,

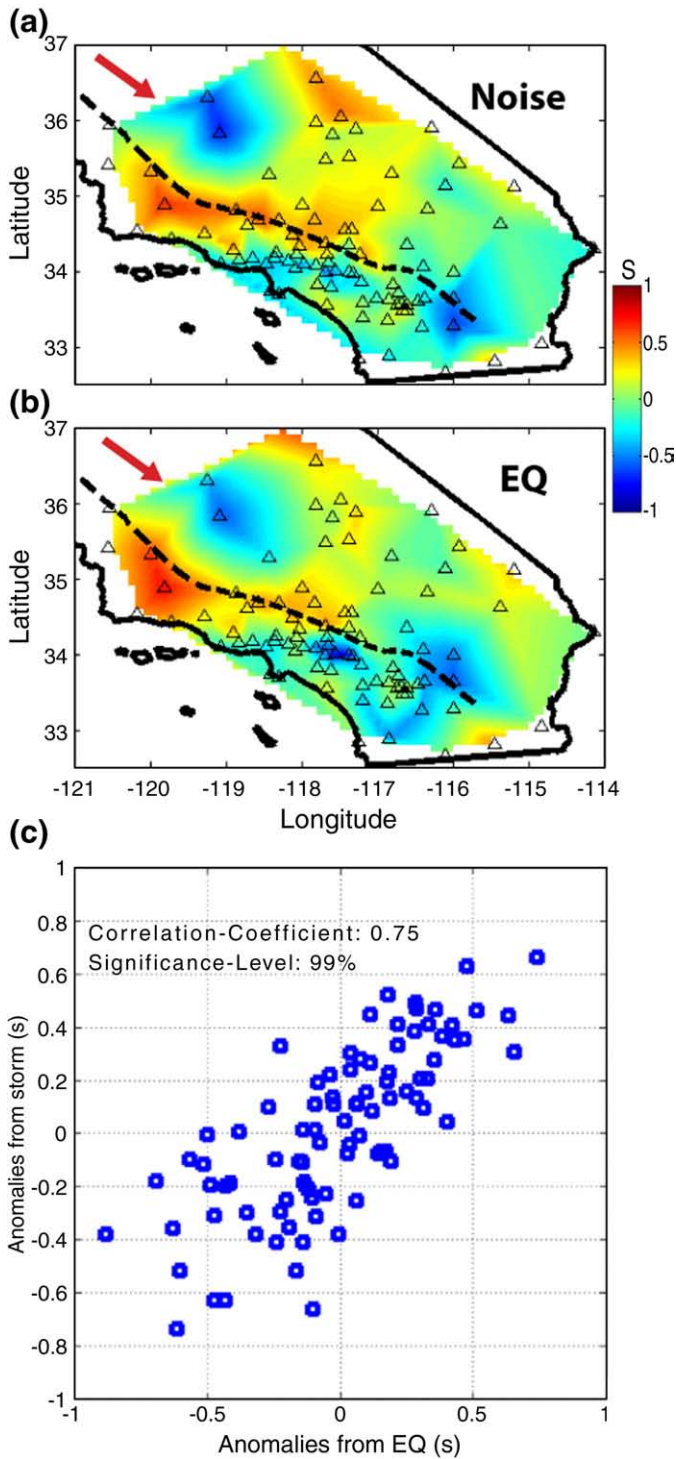


Fig. 8. Comparison of the results from using (a) Super Typhoon Ioke with that from using (b) EQ 2005/11/14, and thus their scatter plot (c), similar to Fig. 7c–e. See Fig. 3e for the storm and earthquake locations.

which requires coherence in a relatively long time-window. An example range-time plot of pulse-like *P*-wave arrivals and the waveform cross-correlation traces (only a fraction) is shown in Fig. 6 for an earthquake near Katrina (EQ 2006/09/10).

We then compare the results obtained from using storms and earthquakes respectively, for the relative *P*-wave arrival-time estimates, and accordingly for the *P*-wave travel-time anomalies as well. Anomalies are calculated as the zero-mean difference between the relative arrival-time estimates and the modeled

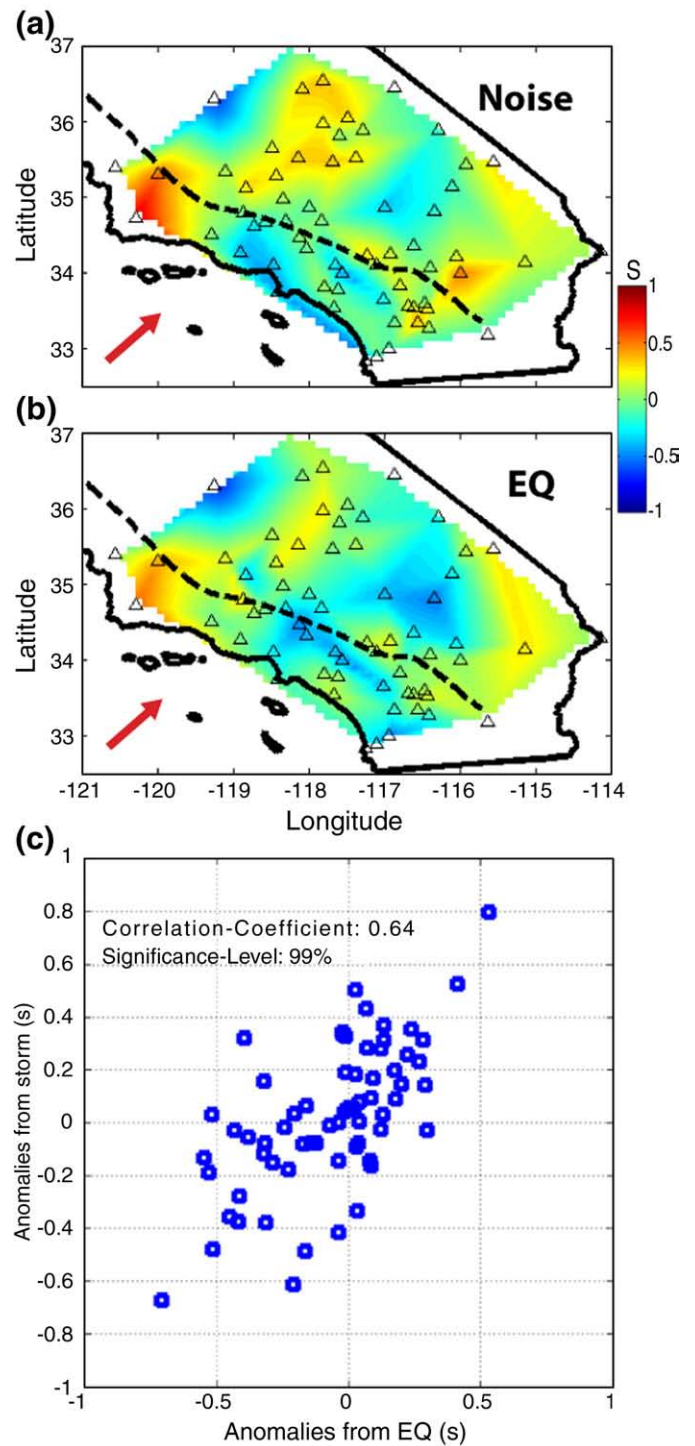


Fig. 9. Comparison of the results from using (a) a South Pacific storm with that from using (b) EQ 2008/10/19, and thus their scatter plot (c), similar to Fig. 7c–e. See Fig. 3e for the storm and earthquake locations.

relative arrival times. Upon choosing a reference arrival-time model, an earthquake can be regarded as a point source and thus the modeled arrival times can be calculated using the earthquake location and a standard Earth model, e.g., *ak135* (Kennett et al., 1995). When using a storm, the source point of its peak *P*-wave energy may be approximated by the location of the peak beam power. Thus the modeled arrival times can be calculated in the same way as is used for an earthquake. Alternatively the azimuth–slowness beam can provide a plane-wave reference model of the

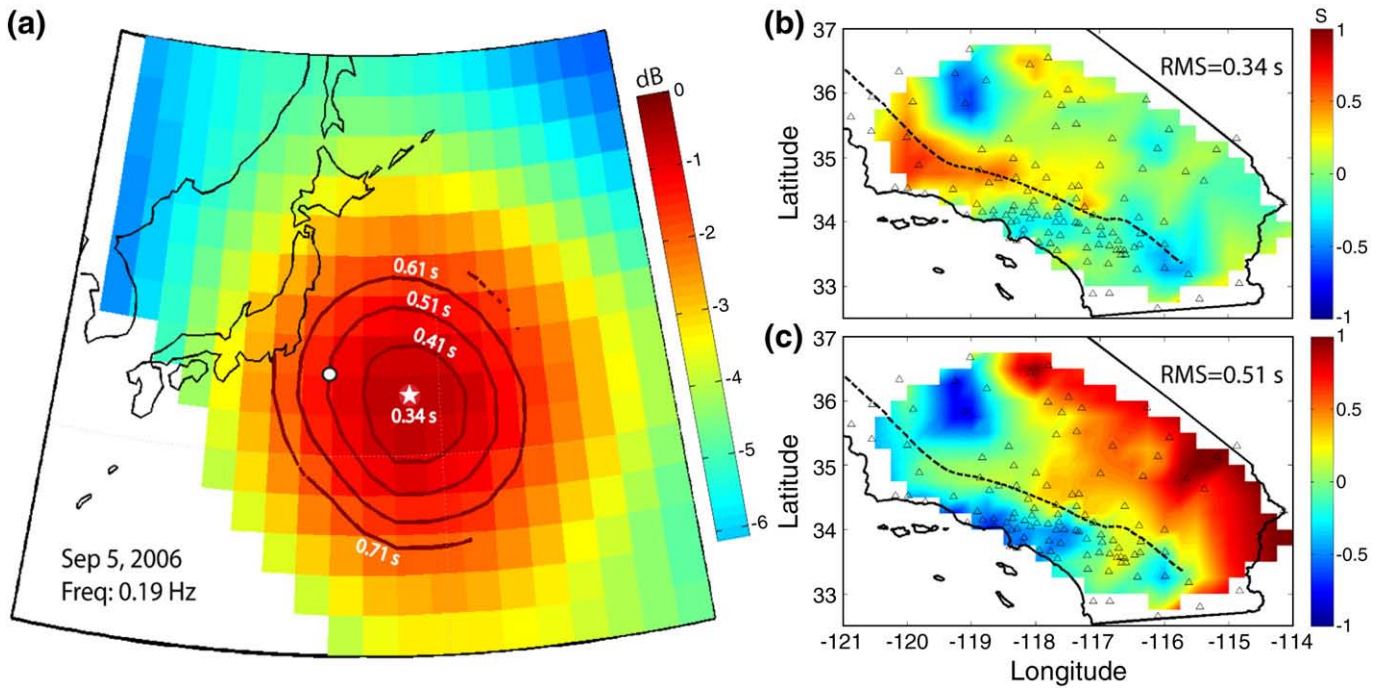


Fig. 10. Point-source representation of a storm. (a) Beamformed source locations of the P -wave microseisms observed at the SCSN on September 5, 2006. Contours are shown for the RMS values of the travel-time anomalies, individually corresponding to using a map point as the P -wave source location. Star marks the peak power location. (b) P -wave travel-time anomalies obtained from using the peak power source location (and the *ak135* model) for calculating the reference travel times. (c) P -wave travel-time anomalies obtained from using an offset point, i.e., the dot in (a), as the source location for calculating the reference travel times.

relative arrival times from a storm, without the need for a precise source location. We have noticed that the two methods result in very similar anomaly patterns (see Section 4).

The first comparison is shown in Fig. 7 for Hurricane Katrina ($\sim 27^\circ$ away from the SCSN) and an Mw 5.9 earthquake that occurred in the Gulf of Mexico on September 10, 2006 (see Fig. 1a for the storm and earthquake locations). The relative P arrival times estimated by using Katrina noise and their residuals relative to a plane-wave arrival (with an apparent speed of 11.8 km/s and a back-azimuth of 100°) are shown in Fig. 7a and c respectively. Similarly, the estimates using the earthquake and their residuals relative to the *ak135*-predicted arrival times are shown in Fig. 7b and d respectively. It can be seen that the travel-time anomalies obtained from using Katrina-generated P waves are well correlated with those from an earthquake in the same source region. For example, the slow anomalies at the Mojave Desert side of the San Andreas Fault (SAF) and the Los Angeles basin (see Fig. 7f for the basic geological features) are observed both from Katrina (Fig. 7c), and EQ 2006/09/10 (Fig. 7d). To quantify this, the correlation coefficient between the two anomaly patterns is 0.62, with a significance level over 99%, calculated by using the noise vs. earthquake anomalies at 80 common stations (see also a scatter plot in Fig. 7e).

We find that this approach also works well for storms at longer distances. The second example is given in Fig. 8 by repeating the above procedure for Super Typhoon Ioke during September 5, 2006, which was $\sim 75^\circ$ away from the SCSN. In Fig. 3a and c, we show the location of Ioke, as indicated respectively by the peak ocean wave hindcast and by the peak P -wave source beam of the seismic noise. Ioke appears in the beamformer output with a slowness of 0.051 s/km (19.6 km/s) and a back-azimuth of 300° . An Mw 7.0 earthquake near Japan on November 14, 2005 (Fig. 3e) is used to show a comparison of its P -wave relative arrival-time estimates with those obtained from using Ioke-generated P waves. Lastly we show in Fig. 9 the anomaly pattern from using a South

Pacific storm ($\sim 78^\circ$ away from the SCSN, see Fig. 3b and d) during July 1, 2006, compared with that from an Mw 6.9 earthquake near Fiji on October 19, 2008 (Fig. 3e). This South Pacific storm appears in the beamformer output with a slowness of 0.05 s/km (20 km/s) and a back-azimuth of 228° . In Figs. 8 and 9 respectively, once again a good correlation between the noise- and earthquake-derived anomaly patterns is directly visible in the map and quantified in the scatter plot. General agreement can be seen over regions such as the Great Valley, the Transverse Ranges, and the Salton Trough, further proving that P -wave travel-time anomalies can be resolved by using storms. Although beyond the scope of this work, one may also notice the large variation of the anomaly pattern obtained from events (either storms or earthquakes) with different directions and/or distances. Across the Salton Trough, for instance, Fig. 8 shows fast anomalies whereas a slow pattern can be seen in Fig. 9. Such differences can be used to image the heterogeneities at depth using tomographic inversion methods.

4. Discussion

In the above comparisons (Figs. 7–9), we model the reference P arrival times from a storm with a plane wave, which is constructed by using the beamformed azimuth and slowness of the P arrivals. Seismic waves arriving from a teleseismic point source to a local/regional array can often be approximated as plane-wave arrivals. Considering that a storm excites energy over a relatively broad source area and is dynamic over time and position, a plane wave representing the direction and speed of the averaged peak arrivals may provide a better fit than shooting rays from a point source. In order to evaluate the choice of a reference model when using a storm, for Super Typhoon Ioke we quantify the relative bias of different sets of the calculated anomalies with their RMS values, and test with different point-source locations within the beamformed P -wave source region, e.g., within the 3-dB beam width

from the peak (see Fig. 10a). It can be seen that the anomalies from using the peak power location as the point source (Fig. 10b, $RMS = 0.34$ s) show a very similar pattern as that from using a plane-wave reference model (Fig. 8a, $RMS = 0.32$ s). This indicates that either using a plane-wave model or using rays from the peak power source point can effectively serve as the reference for calculating the anomalies. However, using a point source offset from the peak power point (e.g., the dot in Fig. 10a), appears to give a biased anomaly pattern (e.g., Fig. 10c). This is also quantified by the RMS contours in Fig. 10a.

The beamformed peak power location of a storm does not necessarily coincide with the storm center (e.g., in Fig. 2). Besides the beamforming bias due to the heterogeneity of Earth structures, there likely is a real shift of the *P*-wave source location from the storm center, since the wave–wave interaction, assumed as the *P*-wave generation mechanism, can occur wherever the opposing waves are developing. For example, the western quadrant of a storm forces wind waves southward. If the storm is moving northward faster than its waves, the currently generated southward wind waves could interact with previously generated northward wind waves at locations behind the storm. The wave–wave interaction may also occur when swells approach the coast and meet with their reflections. In this case the *P*-wave source locations should be closer to the coast than the storm itself.

5. Conclusion

Using the *P*-wave microseisms of pelagic origin recorded in southern California and generated by Hurricane Katrina, Super Typhoon Ioke, and a South Pacific storm, we have extracted accurate relative *P*-wave arrival times. In practice, a candidate storm is analyzed via array beamforming. Once strong *P* waves are identified and characterized, NCC processing is conducted for obtaining the delay times of *P* arrivals between each pair of stations. Determination of relative arrival times is then realized by solving timing residual equations using least squares. The *P*-wave travel-time anomalies derived from distant storms are similar to those obtained from earthquakes close to the storms. This indicates that oceanic storms may contribute to tomography by providing additional teleseismic sources for imaging Earth structure. Improvements in regional body-wave tomography may come from using oceanic sources that can fill azimuthal gaps in the earthquakes recorded in a particular region.

Acknowledgments

This work was supported by the U.S. Air Force Research Laboratory, FA8718-07-C-0005. The seismic data are from the Southern California Seismic Network (SCSN) as distributed through the Southern California Earthquake Data Center (SCEDC).

References

Aki, K., Christofferson, A., Husebye, E.S., 1976. Three-dimensional seismic structure of the lithosphere under Montana LASA. *Bull. Seismol. Soc. Am.* 66, 501–524.

Aki, K., Christofferson, A., Husebye, E.S., 1977. Determination of the 3-dimensional seismic structure of the lithosphere. *J. Geophys. Res.* 82, 277–296.

Efron, B., 1982. The jackknife, the bootstrap, and other resampling plans. SIAM, Philadelphia.

Gerstoft, P., Fehler, M.C., Sabra, K.G., 2006a. When Katrina hit California. *Geophys. Res. Lett.* 33, L17308. doi:10.1029/2006GL027270.

Gerstoft, P., Sabra, K.G., Roux, P., Kuperman, W.A., Fehler, M.C., 2006b. Green's functions extraction and surface-wave tomography from microseisms in southern California. *Geophysics* 71, SI23–SI31.

Gerstoft, P., Shearer, P.M., Harmon, N., Zhang, J., 2008. Global *P*, *PP*, and *PKP* wave microseisms observed from distant storms. *Geophys. Res. Lett.* 35, L23306. doi:10.1029/2008GL036111.

Haubrich, R.A., McCamy, K., 1969. Microseisms: costal and pelagic sources. *Rev. Geophys.* 7, 539–571.

Humphreys, E.D., Clayton, R.W., 1990. Tomographic image of the southern California mantle. *J. Geophys. Res.* 95, 19725–19746.

Husebye, E.S., Christofferson, A., Aki, K., Powell, C., 1976. Preliminary results of the 3-dimensional seismic structure of the lithosphere under the USGS Central California seismic array. *Geophys. J. Roy. Astron. Soc.* 46, 319–340.

Kang, T.S., Shin, J.S., 2006. Surface-wave tomography from ambient seismic noise of accelerograph networks in southern Korea. *Geophys. Res. Lett.* 33, L17303.

Kennett, B.L.N., Engdahl, E.R., Buland, R., 1995. Constraints on seismic velocities in the Earth from travel times. *Geophys. J. Int.* 122, 108–124.

Koper, K., de Foy, B., 2008. Seasonal anisotropy of short-period seismic noise recorded in south Asia. *Bull. Seismol. Soc. Am.* 98, 3033–3045.

Koper, K., de Foy, B., Benz, H.M., 2010. Composition and variation of noise recorded at the Yellowknife seismic array, 1991–2007. *J. Geophys. Res.* doi:10.1029/2008JB006307.

Lacoss, R.T., Kelly, E.J., Toksoz, N.M., 1969. Estimation of seismic noise structure using arrays. *Geophysics* 34, 21–38.

Landes, M., Hubans, F., Shapiro, N.M., Paul, A., Campillo, M., 2010. Origin of deep ocean microseisms by using teleseismic body waves. *J. Geophys. Res.* doi:10.1029/2009JB006918.

Liang, C., Langston, C.A., 2008. Ambient seismic noise tomography and structure of east North America. *J. Geophys. Res.* 113 (B3), B03309. doi:10.1029/2007JB005350.

Lin, F.-C., Ritzwoller, M.H., Townend, J., Bannister, S., Savage, M.K., 2007. Ambient noise Rayleigh wave tomography of New Zealand. *Geophys. J. Int.* 170 (2), 649–666.

Lin, F.-C., Moschetti, M.P., Ritzwoller, M.H., 2008. Surface wave tomography of the western United States from ambient seismic noise: Rayleigh and Love wave phase velocity maps. *Geophys. J. Int.* 173 (1), 281–298.

Moschetti, M.P., Ritzwoller, M.H., Shapiro, N.M., 2007. Surface wave tomography of western United States from ambient seismic noise: Rayleigh wave group velocity maps. *Geochim. Geophys. Geosyst.* 8, Q080101. doi:10.1029/2007GC001655.

Paige, C.C., Saunders, M.A., 1982. LSQR: sparse linear equations and least squares problems. *ACM Transactions on Mathematical Software* 8 (2), 195–209.

Polet, J., 2007. A map of relative *P* wave delay times across southern California. *Geochim. Geophys. Geosyst.* 8, Q10003. doi:10.1029/2007GC001626.

Sabra, K.G., Gerstoft, P., Roux, P., Kuperman, W.A., Fehler, M.C., 2005a. Extracting time-domain Greens function estimates from ambient seismic noise. *Geophys. Res. Lett.* 32, L03310. doi:10.1029/2004GL021862.

Sabra, K.G., Gerstoft, P., Roux, P., Kuperman, W.A., Fehler, M.C., 2005b. Surface wave tomography from microseisms in southern California. *Geophys. Res. Lett.* 32, L14311. doi:10.1029/2005GL023155.

Shapiro, N.M., Campillo, M., 2004. Emergence of broadband Rayleigh waves from correlations of the ambient seismic noise. *Geophys. Res. Lett.* 31, L07614. doi:10.1029/2004GL019491.

Shapiro, N.M., Campillo, M., Stehly, L., Ritzwoller, M.H., 2005. High-resolution surface-wave tomography from ambient seismic noise. *Science* 307, 1615–1617.

Shearer, P.M., 1997. Improving local earthquake locations using the L1 norm and waveform cross correlation: application to the Whittier Narrows, California, after shock sequence. *J. Geophys. Res.* 102, 8269–8283.

Sniieder, R., 2004. Extracting the Green's function from the correlation of coda waves: a derivation based on stationary phase. *Phys. Rev. E* 69, 046610.

Stehly, L., Campillo, M., Shapiro, N.M., 2006. A study of the seismic noise from its long-range correlation properties. *J. Geophys. Res.* 111, B10306. doi:10.1029/2005JB004237.

Toksoz, N.M., Lacoss, R.T., 1968. Microseisms: mode structure and sources. *Science* 159, 872–873. doi:10.1126/science.159.3817.872.

Tolman, H.L., 2005. Manual and wave user system documentation of WAVEWATCH-III. NOAA, Camp Springs, Md. Available at <http://polar.ncep.noaa.gov/>.

Tsai, V.C., 2009. On establishing the accuracy of noise tomography travel-time measurements in a realistic medium. *Geophys. J. Int.* 178 (3), 1555–1564.

VanDecar, J.C., Crosson, R.S., 1990. Determination of teleseismic relative phase arrival times using multi-channel cross-correlation and least squares. *Bull. Seismol. Soc. Am.* 80, 150–169.

Waldhauser, F., Ellsworth, W.L., 2000. A double-difference earthquake location algorithm: method and application to the northern Hayward fault. *California. Bull. Seismol. Soc. Am.* 90, 1353–1368.

Wapenaar, K., 2004. Retrieving the elastodynamic Green's function of an arbitrary inhomogeneous medium by cross correlation. *Phys. Rev. Lett.* 93, 254301.

Yang, Y., Ritzwoller, M.H., 2008. Characteristics of ambient seismic noise as a source for surface wave tomography. *Geochim. Geophys. Geosyst.* 9, doi:10.1029/2007GC001814.

Yang, Y., Ritzwoller, M.H., Levshin, A.L., Shapiro, N.M., 2007. Ambient noise Rayleigh wave tomography across Europe. *Geophys. J. Int.* 168, 259–274.

Yang, Y., Li, A., Ritzwoller, M.H., 2008. Crustal and uppermost mantle structure in southern Africa revealed from ambient noise and teleseismic tomography. *Geophys. J. Int.* 174, 235–248.

Yao, H., van der Hilst, R.D., 2009. Analysis of ambient noise energy distribution and phase velocity bias in ambient noise tomography, with application to SE Tibet. *Geophys. J. Int.* 179, 1113–1132.

Yao, H., van der Hilst, R.D., de Hoop, M.V., 2006. Surface-wave array tomography in SE Tibet from ambient seismic noise and two-station analysis: I – phase velocity maps. *Geophys. J. Int.* 166, 732–744.

Yao, H., Beghem, C., van der Hilst, R.D., 2008. Surface-wave array tomography in SE Tibet from ambient seismic noise and two-station analysis: II – crustal and upper mantle structure. *Geophys. J. Int.* 173, 205–219.

Zhang, J., Gerstoft, P., Shearer, P.M., 2009. High-frequency *P*-wave seismic noise driven by ocean winds. *Geophys. Res. Lett.* 36, L09302. doi:10.1029/2009GL037761.

Zheng, S., Sun, X., Song, X., Yang, Y., Ritzwoller, M.H., 2008. Surface wave tomography of China from ambient seismic noise correlation. *Geochim. Geophys. Geosyst.* 9, Q0502. doi:10.1029/2008GC001981.